
Proceedings Paper:
Ai, S. and Long, H. orcid.org/0000-0003-1673-1193 (2019) Finite element modelling of material deformation and damage by tension under cyclic bending and compression test. In: Galdos, L., Arrazola, P., de Argandoña, E.S., Otegi, N., Mendiguren, J., Madariaga, A. and de Buruaga, M.S., (eds.) Proceedings of the 22nd International Esaform Conference on Material Forming: Esaform 2019. 22nd International Esaform Conference on Material Forming: Esaform 2019, 08-10 May 2019, Vitoria-Gasteiz, Spain. AIP Conference Proceedings, 2113 . AIP Publishing . ISBN 9780735418479

https://doi.org/10.1063/1.5112750

Finite element modelling of material deformation and damage by tension under cyclic bending and compression test

Cite as: AIP Conference Proceedings **2113**, 180012 (2019); https://doi.org/10.1063/1.5112750
Published Online: 02 July 2019

Sheng Ai, and Hui Long

Finite Element Modelling of Material Deformation and Damage by Tension under Cyclic Bending and Compression Test

Sheng Ai[1, a)] and Hui Long[1, b)]

[1] Department of Mechanical Engineering, the University of Sheffield, Sheffield, S1 3JD, UK
[a)] sai1@sheffield.ac.uk
[b)] Corresponding author: h.long@sheffield.ac.uk

Abstract. Material deformation is determined by strain and stress states resulted from loading conditions applied on the material during the manufacturing process. Different testing methods, for example, uniaxial tensile test and dome test have been used to predict material deformation behavior during the manufacturing processes. However, under a complex deformation mode, materials display distinct deformation behavior. In double side incremental forming (DSIF) process, it has been widely acknowledged that the material deformation consists of stretching, bending, shearing, compression with cyclic loading. This leads to a significant material formability enhancement comparing to conventional sheet metal forming processes. This phenomenon cannot be explained by using the currently available testing methods because the complexity of the DSIF process prohibits a direct investigation of the influence of individual deformation modes. To simplify the loading conditions and to investigate their individual and interactive effects contributing to the formability enhancement in DSIF, in this study, a novel testing method of Tension under Cyclic Bending and Compression (TCBC) is proposed, through which the effect of stretching, bending, compression and cyclic loading can be independently evaluated. A finite element (FE) damage modelling of the TCBC test was developed by incorporating the shear-modified Gurson-Tvergaard-Needleman (GTN) model into the Abaqus/Explicit solver. The results showed that the damage accumulation in the material was suppressed due to the localized and cyclic material deformation. An enhanced material formability was obtained by using the FE damage modelling and the periodical accumulation of the damage showed that the TCBC test could be a possible representation of the material deformation in DSIF.

Key words: Damage modelling; GTN model; Tension under cyclic bending and compression test.

1. INTRODUCTION

Material formability varies under different loading conditions. Much higher formability can be achieved in incremental sheet forming (ISF) process than conventional sheet metal forming processes for various materials. In double side incremental forming (DSIF) as shown in Fig.1(a), the localized plastic deformation, caused by a combination of stretching, bending, shearing, compression and cyclic loading, leads to a significant material formability improvement [1, 2]. However, due to the complex contact conditions between the tool and workpiece and their interactions in DSIF it is not feasible to conduct a direct investigation of the effect of individual deformation modes on the material formability. In order to simplify the analysis process of single point incremental forming (SPIF), the continuous bending under tension test (CBT) was conducted by Emmens et al. [3]. In the CBT test, the 3D loading condition in SPIF was simplified into a 2D problem and each deformation mode can be individually adjusted. It was found that bending was the most important factor affecting material formability under CBT loading condition. Compared with SPIF, another supporting tool is deployed in DSIF to provide compression force against the forming tool on the other side of the sheet blank. The introduction of the compression force further improves the material formability as well as process applicability however it further complicates the material deformation. In order to investigate the influence of the various deformation modes on the material formability in DSIF, a novel testing concept, named as Tension under Cyclic Bending and Compression (TCBC) test was modelled by Ai et al. [4], as shown in Fig.1(b). Compared with the CBT test, five factors can be individually adjusted in the TCBC test, including

Proceedings of the 22nd International ESAFORM Conference on Material Forming
AIP Conf. Proc. 2113, 180012-1–180012-6; https://doi.org/10.1063/1.5112750
Published by AIP Publishing. 978-0-7354-1847-9/$30.00

stretching speed, bending depth, cyclic stroke speed, compressive force and specimen thickness, reflecting the influence of the key deformation modes in DSIF.

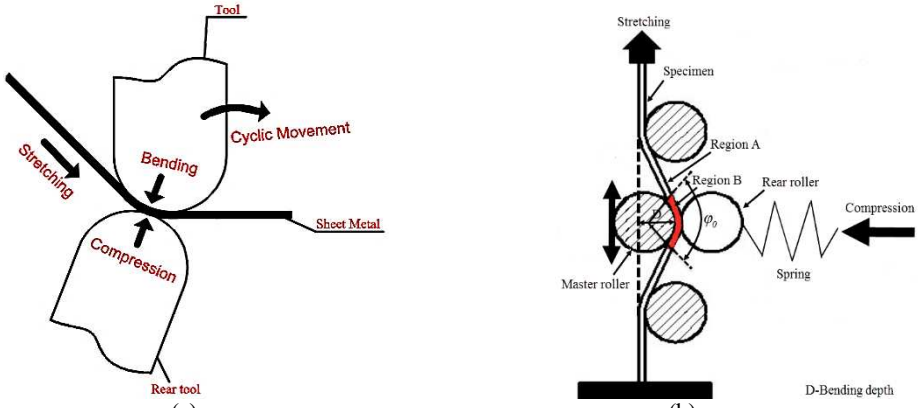

FIGURE 1. (a) Schematic of various deformation modes in DSIF; (b) Schematic of TCBC test concept [4]

Although the TCBC test has enormously simplified the analysis of the material deformation in DSIF, the experimental test itself does not facilitate a direct observation of the material deformation history of the tested area by using techniques such as the digital image correlation (DIC) because both sides of the contact area are covered by the moving tools. Finite element (FE) method is effective and efficient to investigate the deformation history of sheet metal forming processes. The strain and stress distributions and other process-related target variables can be obtained with the deformation history thus providing a comprehensive analysis of the material deformation process. Reported by Malhotra et al.[5], the occurrence of material fracture in ISF has been postponed even though multiple necking has already been formed in the deformed wall of the ISF part.

Various damage models have been proposed to assess the damage level of material in forming processes. Malhotra et al. [5] formulated Xue's damage model [6] into the commercial FE software LS-DYNA to predict the failure in SPIF, incorporating the effect of shear mechanism and stress triaxiality. While Mirnia and Shamsari [7] used the modified Mohr-Coulomb (MMC3) ductile criterion, taking nonlinear loading history into consideration. The selection of the damage model in the FE modelling is crucial in order to produce accurate results to model damage development. Malcher et al. [8] compared four most adopted damage models under various magnitudes of stress triaxiality. Both the GTN model with a shear mechanism and the Lemaitre model attained a better accuracy in predicting damage evolution under low stress triaxiality states than that by the Bai-Wierzbick model. All four models achieved very good accuracy in predicting damage under high and moderate stress triaxiality states.

In this study, the GTN model with Nahshon-Hutchinson shear mechanism was used to model the material deformation and damage evolution in the TCBC test. In the following sections, the shear-modified GTN model was first introduced, followed by the identification of the key parameter values of the damage model. By incorporating the damage model into Abaqus/Explicit solver, a FE simulation of the TCBC test was conducted and the damage evolution during the testing process was analyzed.

2. DAMAGE MODELLING OF THE TCBC TEST

2.1 Introduction to the GTN Damage Model

GTN model is a micro void evolution yielding criterion based on the Gurson model [9], which was further improved by Tvergaard [10], Needleman and Rice [11], and Chu and Needleman [12],

$$\Phi = \left(\frac{\sigma_{eq}}{\sigma_0}\right)^2 + 2q_1 f^* cosh\left(-\frac{3q_2\sigma_m}{2\,\sigma_0}\right) - (1 + q_3 f^{*2}) = 0 \quad (1)$$

Where σ_{eq} is the microscopic equivalent plastic stress, σ_0 is the macroscopic flow stress, and σ_m is the hydrostatic stress. The parameters q_1, q_2 and q_3 are used to describe the interactive effect between the existing voids, and $q_3 = q_1^2$. The values determined by Tvergaard [10] may be used in the GTN model, in which $q_1 = 1.5, q_2 = 1$ and $q_3 = 2.25$. In GTN model, the severity of the damage is assessed by the void volume fraction (VVF) f. When f reaches f_f, material fracture occurs. To compensate for the rapid closure of voids upon fracture, f^* is introduced by Tvergaard and Needleman [10, 12] as a function of f,

$$f^* = \begin{cases} f & f \le f_C \\ f_C + k_f \cdot (f - f_C) & f \ge f_C \end{cases} \quad (2)$$

Where k_f is a constant determined by the void volume fractions f_f and f_C,

$$k_f = \frac{f_u^* - f_C}{f_f - f_C}$$

In which f_u^* is defined by,

$$f_u^* = \frac{q_1 + \sqrt{q_1^2 - q_3}}{q_3}$$

To enable the application of GTN model for processes under relatively low stress triaxiality, the additional shear contribution to the void volume growth has been introduced to the GTN model by researchers in addition to the growth of existing voids and the nucleation of the new voids. Nahshon and Hutchinson [13] extension was used in this study for modeling TCBC test. As a result, the growth of the void volume fraction is a contribution from three factors,

$$\dot{f} = \dot{f}_g + \dot{f}_n + \dot{f}_s \quad (3)$$

$$\dot{f}_g = (1 - f)\dot{\varepsilon}_{kk}^P \qquad \dot{f}_n = A\dot{\varepsilon}^p + B\dot{\sigma}_m \qquad \dot{f}_s = k_w \cdot f \cdot w(\sigma) \cdot \frac{s_{ij} \cdot \dot{\varepsilon}_{kk}^P}{\sigma_{eq}} \quad (4)$$

Where $\dot{\varepsilon}_{kk}^P$ is the plastic strain rate tensor, $\dot{\varepsilon}^p$ is the equivalent plastic strain rate, k_w and $w(\sigma)$ are shear related components, and s_{ij} is the deviatoric stress tensor.

Based on the mathematical expressions, the numerical discretization of the GTN model can be realized. Stress and strain components and the process-related state variables can be updated with the help of the backward-Euler numerical algorithm proposed by Simo and Hughes [14], which was first applied into the GTN model by Aravas [15]. In this algorithm, an elastic stress predictor is first calculated based on Hooke's Law, the predicted stress components will be used to check whether the yielding criterion is met. If not, the elastic predictor will be the final stress to be updated. Otherwise, a plastic correction to the elastic predictor will be made. In this study, the shear-modified GTN model was incorporated into the FE solver Abaqus/Explicit using VUMAT subroutine.

2.2 Calibration of the GTN Model Parameters

According to the Equations (2) and (4), values of five parameters need to be identified in the shear-modified GTN model, including the void volume fraction related parameters f_0, f_C, f_f, f_n and shear related parameter k_w.

Material AA5251-H22 was used in the test and to obtain the mechanical behavior of the material the uniaxial tensile test was performed. The geometry of the tensile specimen is shown in Fig. 2(a) as well as the obtained true plastic strain-true plastic stress curve. In order to describe its deformation behavior under large plastic deformation, different hardening laws, including the Ludwik law, the Voce law and the Swift law were fitted against the obtained true strain-true stress curve. The Voce law was shown to agree the best with the experimental data so that it was used to predict material deformation under large deformation in this study, as shown in Fig. 2(a).

TABLE 1. Limits of the GTN parameters investigated for AA5251-H22

Coefficients	Minimum values	Maximum values
f_0	0.0001	0.005
f_n	0.01	0.05
f_c	0.01	0.05
f_f	0.01	0.1

For f_0, f_C, f_f and f_n, an inverse method has been developed [16, 17]. In the simplest form of the inverse method, multiple trials using the uniaxial tensile test with different combinations of various values of the GTN parameters are run in the FE simulation and the set of the parameters providing the best fit to the experimental results will be treated as the optimal values. In this study, the response was defined as the accumulation of the difference between the forces obtained from the FE simulations and the experiment during the uniaxial tensile test,

$$R = \sum_{i=1}^{n} \left| F_{exp}^i - F_{num}^i \right| \quad (5)$$

According to the publications on the GTN model used for various aluminum alloys, the investigated limits of the parameters for AA5251-H22 were determined, as shown in Table 1.

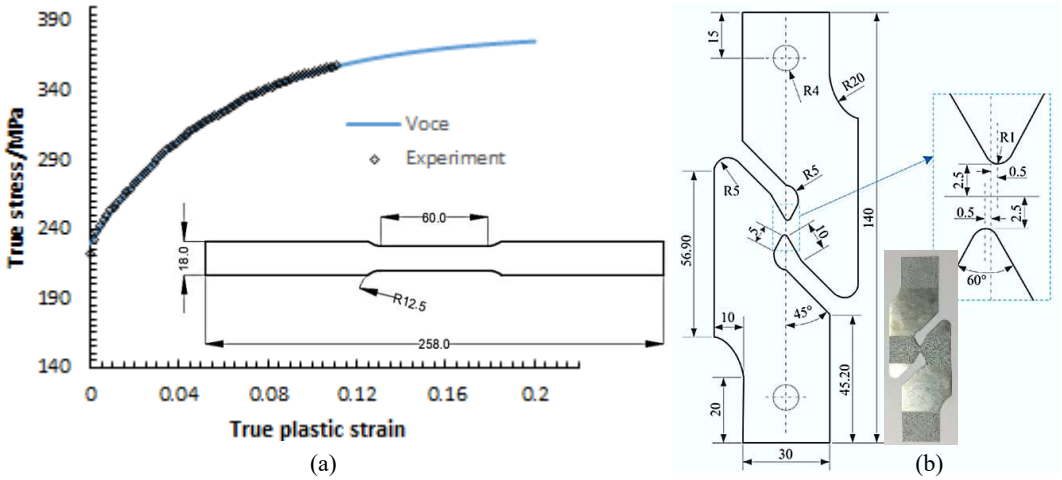

FIGURE 2. Tests to obtain GTN coefficients for AA5251-H22: (a) Plastic strain-stress curve fitting and the prediction by the Voce law - uniaxial tensile test; (b) Pure-shear specimen proposed by Sun et al. [18] - pure shear test

Using central composite design (CCD) method, a quadratic regression relationship between the response and the investigated GTN parameters was obtained. Using the genetic algorithm provided by the software Matlab, the optimized set of the parameters was obtained by minimizing the value of the response,

$$f_0 = 0.002, \qquad f_n = 0.01, \qquad f_c = 0.026, \qquad f_f = 0.044$$

In order to calibrate the shear coefficient k_w, a shear test was performed by using the pure shear specimen proposed by Sun et al. [18], as shown in Fig. 2(b). By varying the value of the parameter k_w from 1 to 2, the displacement-loading force curves was obtained, and it was confirmed that the curve acquired from $k_w = 1.5$ provided the most satisfactory match to the experimental curve. As a result, k_w was determined to be 1.5.

2.3 Finite Element Damage Modelling of the TCBC Test

After obtaining the parameter values required by the damage model, the FE model of the TCBC test was established in the Abaqus/Explicit solver, as shown in Fig.3.

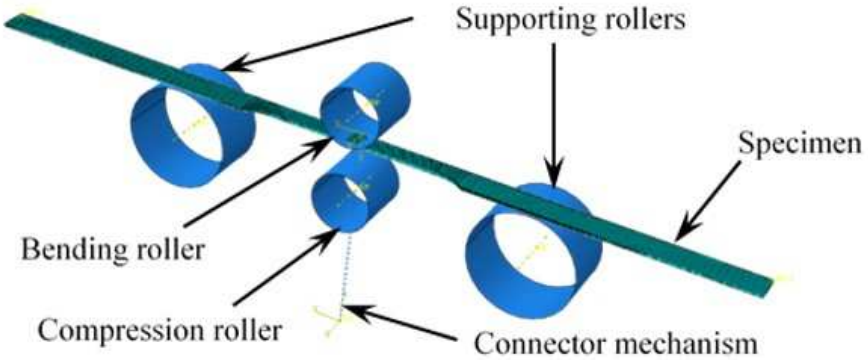

FIGURE 3. FE model of the TCBC test

The specimen with the same dimension in the uniaxial tensile test was used in the FE modelling. The bending depth was set to be 9 mm, compression force was set to be 600 N, the tensile speed was 2.4 mm/min, while the stroke speed of the rollers was set to be 2.5 mm/s and the specimen thickness was 1 mm. The compressive force was applied by using a spring to maintain the contact between the compression roller and the specimen. The spring was defined by the axial connector mechanism provided by Abaqus. Element type C3D8R was used in the model. The element size of central test zone was meshed to be 0.5 mm while the rest was 2 mm. To detect the bending effect, the specimen was meshed to be five layers in the thickness direction. Only half of the specimen was modelled to save the computational power. In the beginning of the modelling process, both ends of the specimen were fixed and the bending roller bent the specimen to the desired bending depth. Then the bending depth was kept constant and fixture at one end of the specimen was released to allow the stretching deformation of the

specimen, after which the cyclic movement of the rollers and stretching from that end of the specimen was started at the same time. The simulation would be terminated as soon as the fracture occurred.

3. RESULTS AND DISCUSSION

The simulation was terminated automatically when the damage indicator, the state variable VVF (SDV2) in several elements had reached f_f. The total computational time was 649.4 seconds, when the specimen reached the maximum elongation of 25.98 mm. Compared with uniaxial tensile test, in which the maximum elongation for the material AA5251-H22 using the same specimen was 9.2 mm, it is clear that the material formability under TCBC condition was significantly enhanced.

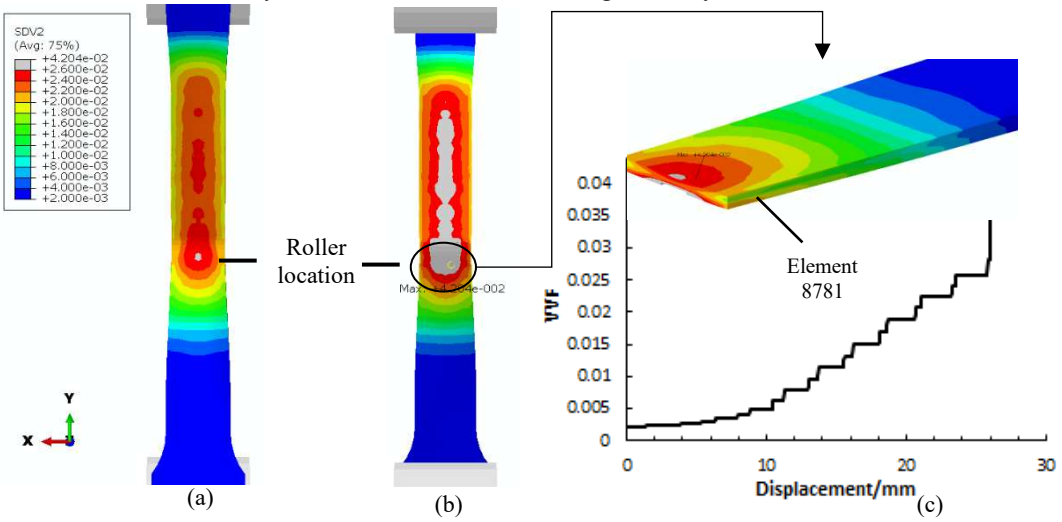

FIGURE 4. Distribution of void volume fraction in the specimen upon fracture: (a) concave surface; (b) convex surface; (c) cross-section of the specimen at the fracture location and accumulation of void volume fraction of element 8781

The distribution of the VVF from both the concave and convex surfaces of the specimen upon the final fracture is shown in Fig. 4. Comparing Fig. 4(a) and (b), it is obvious that the elements on the convex side of the specimen generally received higher damage than those on the concave side. A large portion of the elements on the convex side had already reached the fracture limit while the majority of those on the concave side were still safe, which suggests the existence of bending effect. A clearer image of VVF across the damaged cross-section is shown in Fig.4(c).

FIGURE 5. A comparison of the untested and fractured specimens from uniaxial tensile test and TCBC test

Strong localized deformation was also observed from the simulation results. As shown in Fig.4, several potentially weak zones existed before the final fracture. The fracture only happened when the rollers were in contact with the damaged zone lead to the crack propagation. The accumulation history of VVF of element 8781 on the damaged convex surface is shown in Fig.4(c). It is obvious that the growth of VVF in the element only occurred when the compression roller and the bending roller were in contact with that part of the specimen, which is quite similar to the localized deformation feature in DSIF. However, in the TCBC experimental tests using the same set of parameters, the averaged maximum elongation of the specimen was 34.6 mm, which was 8.62 mm greater than FE prediction, a comparison between the fractured specimens in the uniaxial tensile test and the TCBC test is shown in Fig.5. The early fracture predicted by the FE model can be attributed to the inability of the GTN related models to simulate the material deformation under the low or negative stress triaxiality conditions [8].

4. CONCLUSION

In this study, FE damage modelling of the TCBC test using the GTN-shear modified damage model has been performed. It was found that higher material formability could be achieved under TCBC loading condition than the uniaxial tensile condition. Strong bending effect was shown by comparing the damage distribution across the specimen thickness direction. Stair-like accumulation of the damage presented by void volume fraction was observed which revealed the localized deformation characteristics in the TCBC test, enabling the TCBC test to be a possible representation of the material deformation in DSIF process. In addition, the shear-modified GTN model predicted an early fracture in the TCBC FE damage simulation suggesting that an improved damage model taking into account of the low or negative stress triaxiality would lead a better prediction.

REFERENCES

1. Emmens, W.C. and A.H. van den Boogaard, *An overview of stabilizing deformation mechanisms in incremental sheet forming.* Journal of Materials Processing Technology, 2009. **209**(8): p. 3688-3695.
2. Lu, B., et al., *Investigation of material deformation mechanism in double side incremental sheet forming.* International Journal of Machine Tools and Manufacture, 2015. **93**: p. 37-48.
3. Emmens, W.C. and A.H. van den Boogaard, *Incremental forming by continuous bending under tension—An experimental investigation.* Journal of materials processing technology, 2009. **209**(14): p. 5456-5463.
4. Ai, S., B. Lu, and H. Long, *An analytical study of new material test method for tension under bending and compression in double side incremental forming.* Procedia Engineering, 2017. **207**: p. 1982-1987.
5. Malhotra, R., et al., *Mechanics of fracture in single point incremental forming.* Journal of Materials Processing Technology, 2012. **212**(7): p. 1573-1590.
6. Xue, L., *Damage accumulation and fracture initiation in uncracked ductile solids subject to triaxial loading.* International journal of solids and structures, 2007. **44**(16): p. 5163-5181.
7. Araghi, B.T., et al., *Review on the development of a hybrid incremental sheet forming system for small batch sizes and individualized production.* Production Engineering, 2011. **5**(4): p. 393-404.
8. Malcher, L., F.A. Pires, and J.C. De Sá, *An assessment of isotropic constitutive models for ductile fracture under high and low stress triaxiality.* International Journal of Plasticity, 2012. **30**: p. 81-115.
9. Gurson, A.L., *Continuum theory of ductile rupture by void nucleation and growth: Part I—Yield criteria and flow rules for porous ductile media.* Journal of engineering materials and technology, 1977. **99**(1): p. 2-15.
10. Tvergaard, V., *Influence of voids on shear band instabilities under plane strain conditions.* International Journal of fracture, 1981. **17**(4): p. 389-407.
11. Needleman, A. and J. Rice, *Limits to ductility set by plastic flow localization*, in *Mechanics of sheet metal forming*. 1978, Springer. p. 237-267.
12. Chu, C. and A. Needleman, *Void nucleation effects in biaxially stretched sheets.* Journal of engineering materials and technology, 1980. **102**(3): p. 249-256.
13. Nahshon, K. and J. Hutchinson, *Modification of the Gurson model for shear failure.* European Journal of Mechanics-A/Solids, 2008. **27**(1): p. 1-17.
14. Simo, J.C. and T.J. Hughes, *Computational inelasticity*. Vol. 7. 2006: Springer Science & Business Media.
15. Aravas, N., *On the numerical integration of a class of pressure‐dependent plasticity models.* International Journal for numerical methods in engineering, 1987. **24**(7): p. 1395-1416.
16. Kami, A., et al., *Numerical determination of the forming limit curves of anisotropic sheet metals using GTN damage model.* Journal of Materials Processing Technology, 2015. **216**: p. 472-483.
17. Ying, L., et al., *On the numerical implementation of a shear modified GTN damage model and its application to small punch test.* International Journal of Material Forming, 2018. **11**(4): p. 527-539.
18. Sun, Q., et al., *Analysis of edge crack behavior of steel sheet in multi-pass cold rolling based on a shear modified GTN damage model.* Theoretical and Applied Fracture Mechanics, 2015. **80**: p. 259-266.